Wind and Structures, *Vol. 30, No. 6 (2020) 575-595*
DOI: https://doi.org/10.12989/was.2020.30.6.575

Observational study of wind characteristics from 356-meter-high Shenzhen Meteorological Tower during a severe typhoon

Yinghou He[1,2], Qiusheng Li*[1,2] Pakwai Chan[3], Li Zhang[4], Honglong Yang[4] and Lei Li[4]

[1]*Department of Architecture and Civil Engineering, City University of Hong Kong, Kowloon, Hong Kong*
[2]*Architecture and Civil Engineering Research Center, Shenzhen Research Institute of City University of Hong Kong, Shenzhen, China*
[3]*Hong Kong Observatory, Kowloon, Hong Kong*
[4]*Shenzhen National Climate Observatory, Shenzhen, China*

(*Received September 26, 2019, Revised March 27, 2020, Accepted April 25, 2020*)

Abstract. The characteristics of winds associated with tropical cyclones are of great significance in many engineering fields. This paper presents an investigation of wind characteristics over a coastal urban terrain based on field measurements collected from multiple cup anemometers and ultrasonic anemometers equipped at 13 height levels on a 356-m-high meteorological tower in Shenzhen during severe Typhoon Hato. Several wind quantities, including wind spectrum, gust factor, turbulence intensity and length scale as well as wind profile, are presented and discussed. Specifically, the probability distributions of fluctuating wind speeds are analyzed in connection with the normal distribution and the generalized extreme value distribution. The von Karman spectral model is found to be suitable to depict the energy distributions of three-dimensionally fluctuating winds. Gust factors, turbulence intensity and length scale are determined and discussed. Moreover, this paper presents the wind profiles measured during the typhoon, and a comparative study of the vertical distribution of wind speeds from the field measurements and existing empirical models is performed. The influences of the topography features and wind speeds on the wind profiles were investigated based on the field-measured wind records. In general, the empirical models can provide reasonable predictions for the measured wind speed profiles over a typical coastal urban area during a severe typhoon.

Keywords: field measurement; wind characteristics; typhoon; meteorological tower

1. Introduction

Wind characteristics in the atmospheric boundary layer (ABL) have received much attention over the last few decades due to their applications in many fields of engineering. Numerous studies have attempted to explore the wind characteristics in the ABL by field measurements or observations, particularly in connection with tropical cyclone winds (Roth 2000, Eliasson *et al*. 2006, Shu *et al*. 2017). Vertical wind profiles and atmospheric turbulence properties, such as energy spectra, turbulence intensities and gust factors of wind velocity are regarded as typical ABL characteristics. Significant efforts have been made to investigate the ABL characteristics based on measurements from numerous heights over different terrain conditions (Shiau and Chen 2002, Tamura *et al*. 2007, Schroeder *et al*. 2009, He *et al*. 2013b, Hoebbel *et al*. 2018, Peng *et al*. 2018). Specifically, several models were proposed with respect to these items, e.g., various power spectral forms proposed by von Karman (1948), Davenport (1960) and Kaimal *et al*. (1972), empirical formulas for gust factors proposed by Ishizaki (1983) and Cao *et al*. (2009) and guidelines for turbulence intensity recommended by AIJ (1996) and ASCE (1998). However, a literature review reveals that previous studies were mostly concerned with wind profiles and atmospheric turbulence properties over open flat or relatively smooth terrains, while investigations of wind profiles and atmospheric turbulence characteristics over urban terrain or built-up areas are still lacking. In particular, there are relatively few reliable observations during strong windstorms such as tropical cyclones. So, there is an urgent need to accumulate such information and knowledges for the wind-resistant design of high-rise buildings. In response to this need, this paper investigates the wind profiles and atmospheric turbulence characteristics through analysis of the wind measurements from numerous anemometers installed at 13 height levels on a 356-m high meteorological tower over a coastal urban area in Shenzhen during a severe typhoon.

Wind profiles depend on various parameters or factors, such as the upwind terrain conditions, the ground surface roughness, atmospheric stability, etc. (Ishizaki 1983, Amano *et al*. 1999, Knupp *et al*. 2000, Kepert 2006, Giammanco 2013). Vickery *et al*. (2009) used a fitting technique of GPS dropsonde wind profiles to model the shape of the vertical profiles of mean horizontal wind speeds in the hurricane boundary layer and estimate surface winds over both marine and land surfaces. Song *et al*. (2012) stated that there were salient differences among wind speed profiles during different typhoon stages based on their field measurement study during Typhoon Hagupit. On one hand, Tse *et al*. (2013) compared the measured profiles of tropical cyclone winds with several empirical models and showed that both the logarithmic law and the power law models could give a

*Corresponding author, Chair Professor
E-mail: bcqsli@cityu.edu.hk

http://www.techno-press.com/journals/was&subpage=7
ISSN: 1226-6116 (Print), 1598-6225 (Online)

reasonable description for the distribution of mean wind speed up to 300 m. He *et al*. (2013a) examined the dependence of wind profiles on different upwind terrain conditions, which indicated for both hilly upwind terrain and open sea upwind terrain, the logarithmic law and the power law could be used to approximately predict wind speed profiles up to 500 m. On the other hand, given the existence of the super-gradient-wind region where the tangential winds are larger than the gradient wind, the log-law or power-law wind profiles under near-neutral conditions may be inappropriate to characterize the ABL winds associated with hurricanes. For example, Snaiki and Wu (2018) developed a semi-empirical model for mean wind speed profile of landfall hurricanes, which consists of a logarithmic function and an empirical function. Consequently, this paper presents the measured profiles considering the influences of topography features and wind speeds by grouping them with different azimuths and magnitudes of wind speed and investigates the differences among those results. Moreover, a comparative study of vertical wind profiles derived from the field measurements of the present study and empirical models is carried out.

The paper is organized as follows: Section 2 introduces the field measurement arrangement, Typhoon Hato and the 356-m meteorological tower in Shenzhen. The following section focuses on analysis of the wind characteristics with respect to wind speed and direction, energy distribution, gust factor, turbulence intensity and length scale as well as wind profiles during the typhoon. The results derived from the field measurements are presented and discussed, and comparisons with existing models and design guidelines are made. Finally, the main findings and conclusions of this observational study are summarized in Section 4.

2. Introduction of Typhoon Hato, meteorological tower and measurement system

As reported by the Hong Kong Observatory, Hato was one of the strongest and most persistent windstorms during the Pacific typhoon season in 2017. Fig. 1(a) shows that Hato originated from a tropical depression over the Western North Pacific, followed a northwesterly track and intensified into a typhoon, then made landfall over the coastal area of Macau (near Shenzhen) at a severe typhoon strength level, and finally dissipated rapidly as it moved further inland. Fig. 1(b) shows the surrounding terrain conditions around the meteorological tower in Shenzhen. Based on the time lines indicated in Fig. 1(a) regarding the typhoon's influence at the observation site, the wind measurements adopted in this paper commenced at 17:00:00 on 22 August 2017 (Beijing Time) and ended at 14:00:00 on 24 August 2017, which covered the main passage process corresponding to the severe winds in Shenzhen during Typhoon Hato.

The Shenzhen Meteorological Tower (SMT), with a height of 356 m, is located in south central Shenzhen. Its base is at a height of 46.5 m above mean sea level (AMSL). The terrain conditions surrounding the SMT feature a coastal urban landscape characterized by buildings, trees and even mountains, as shown in Fig. 1(b). The tower site is surrounded by a number of tall buildings located approximately 3 km to the south, while primarily low-rise buildings are distributed to the northeast approximately 3 km from the tower's location. Towards the north, the area is covered by a mixture of trees and some low-rise residential houses. There is a mountain with a peak of 587 m to the east, and an airport to the west of the tower.

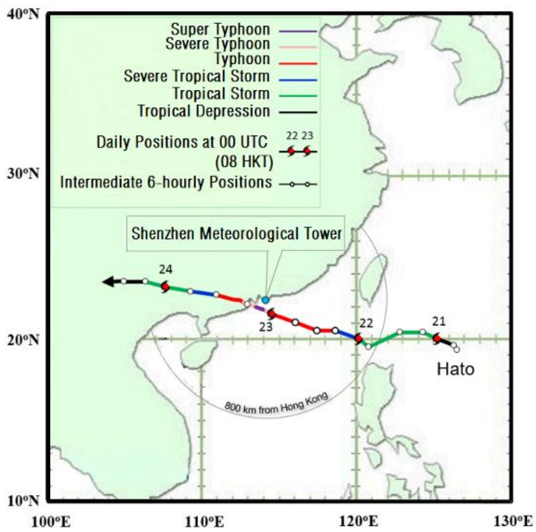

(a) Track of Hato: 20 - 24 August 2017

(b) Surrounding terrain conditions of Shenzhen Meteorological Tower (SMT)

Fig. 1 Track of Typhoon Hato approaching Shenzhen

Thirteen WA-25 cup anemometers (VAISALA, Finland) were installed on the tower at thirteen levels, with heights of 10 m, 20 m, 40 m, 50 m, 80 m, 100 m, 150 m, 160 m, 200 m, 250 m, 300 m, 320 m and 350 m (see Fig. 2), to measure the mean wind speed and direction at a sampling frequency of 0.1 Hz in combination with the mechanical distance constant of 2.7 meters. In addition, four WMT-703 ultrasonic anemometers (VAISALA, Finland) were mounted at 10-, 40-, 160- and 320-m-high levels to record three-dimensional mean and fluctuating wind speeds with a sampling frequency of 10 Hz. The coordinate system for the analysis of mean and turbulent winds is shown in Fig. 2(b).

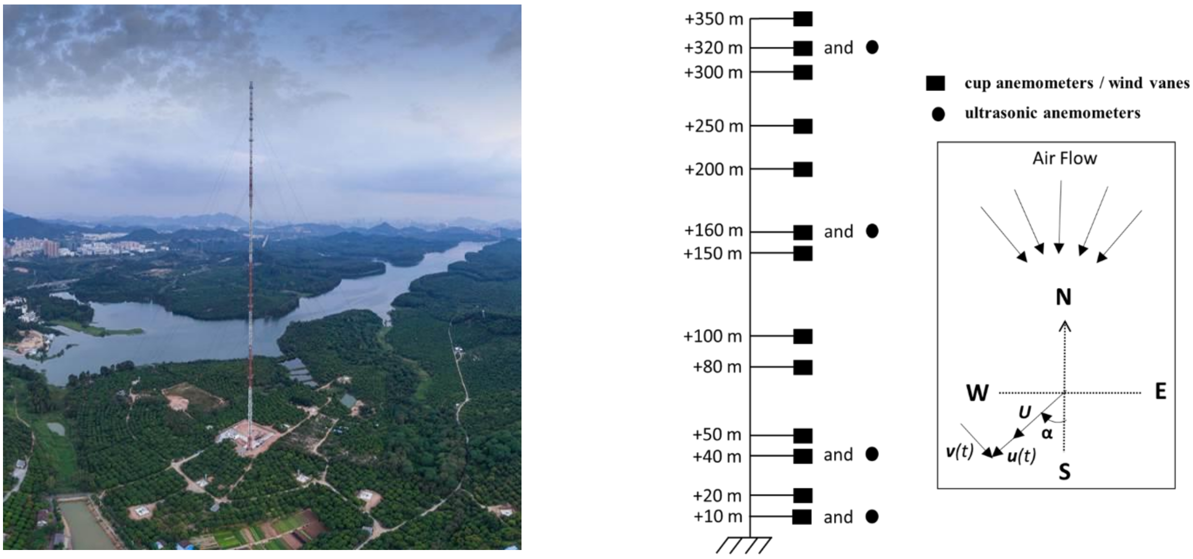

(a) Location of SMT (b) Deployment of anemometers

Fig. 2 Location of SMT and deployment of anemometers

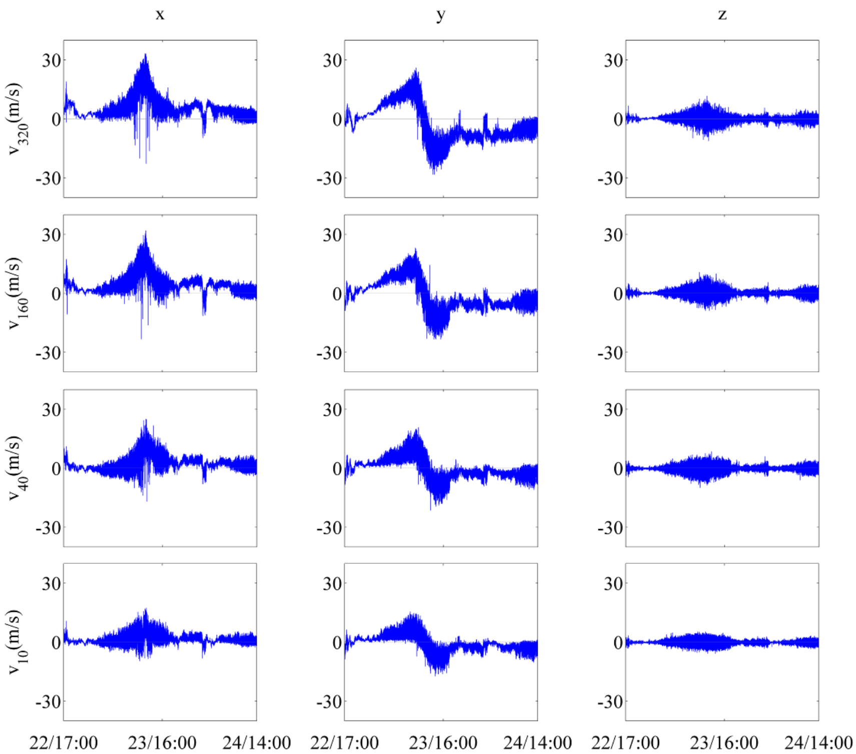

Fig. 3 Time histories of the three orthogonal wind components (Time form at: day/hour: minute, hereafter)

The angle α of the mean wind direction is positive clockwise and north is defined as 0°.

3. Wind characteristics

In this section, the wind records from the anemometers at all 13 heights along the mast are used to investigate the wind characteristics during Typhoon Hato. Specifically, the wind records from the four ultrasonic anemometers located at 10 m, 40 m, 160 m and 320 m heights are used to investigate the characteristics of atmospheric turbulence such as spectrum, gust factor and turbulence intensity during the typhoon, while the measurements from both the cup anemometers/wind vanes and ultrasonic anemometers installed at all 13 heights are used to determine the vertical wind profiles which are compared with empirical models.

3.1 Wind speed and direction

3.1.1 Time history of measured wind records

Time histories of the wind measurements from the

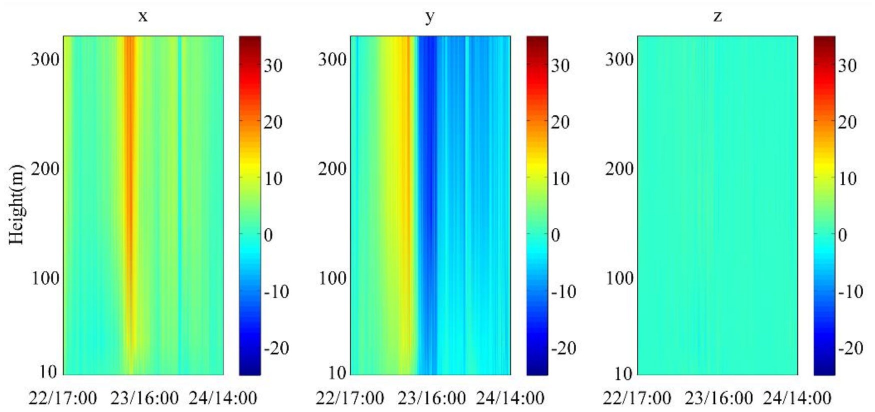

Fig. 4 Filled color contour of three orthogonal wind components

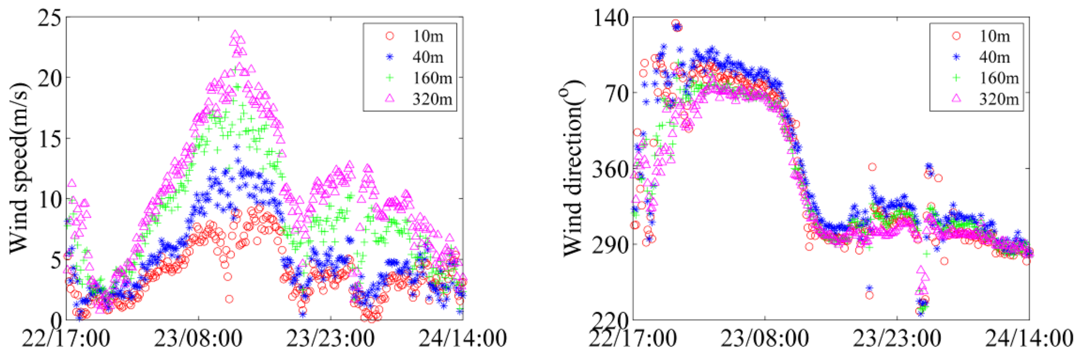

Fig. 5 Time history of 10-min mean horizontal wind speed

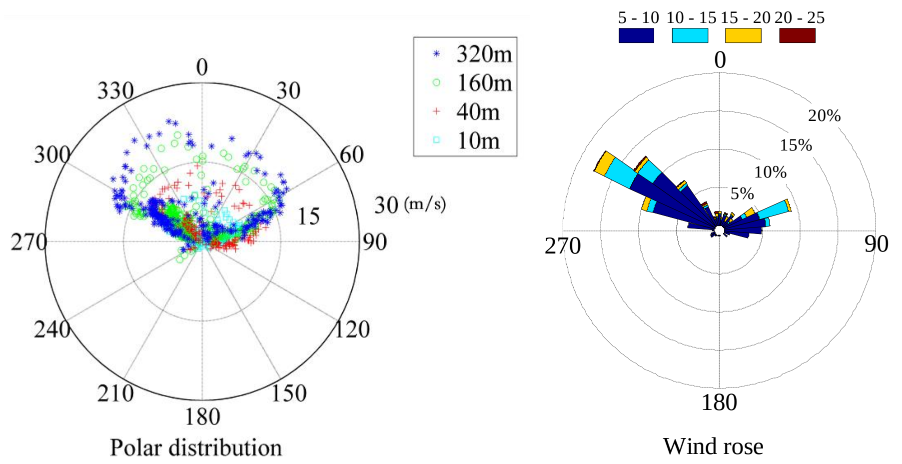

Fig. 6 Polar distribution and wind rose of 10 m in mean horizontal wind speed

ultrasonic anemometers at the four heights from 17:00 on August 22 to 14:00 on August 24 are shown in Fig. 3. This period covered the main passage process when Hato came close to Shenzhen or corresponded to the most severe winds during the typhoon. In this paper, the wind records during this selected period are used in the following analysis, unless otherwise stated. Variations in wind speed at different heights for both horizontal components in the east-west (x) and north-south (y) directions, and the vertical component (z direction) show consistent change trends, in which the wind speed increased continuously as the typhoon approached the observation station; the wind speed reached its peak value at approximately 13:00 on August 23, achieving the maximum speed of 33.3 m/s in the horizontal east-west direction and 11.6 m/s in the vertical direction at the height of 320 m, and the speed decreased gradually as the typhoon moved away from the measurement site. For convenience of illustration along the whole height, the wind history evolution is shown in Fig. 4 in filled color contour form. The strip of maximum wind in the x direction indicates the shortest distance from the typhoon's center to the observation site.

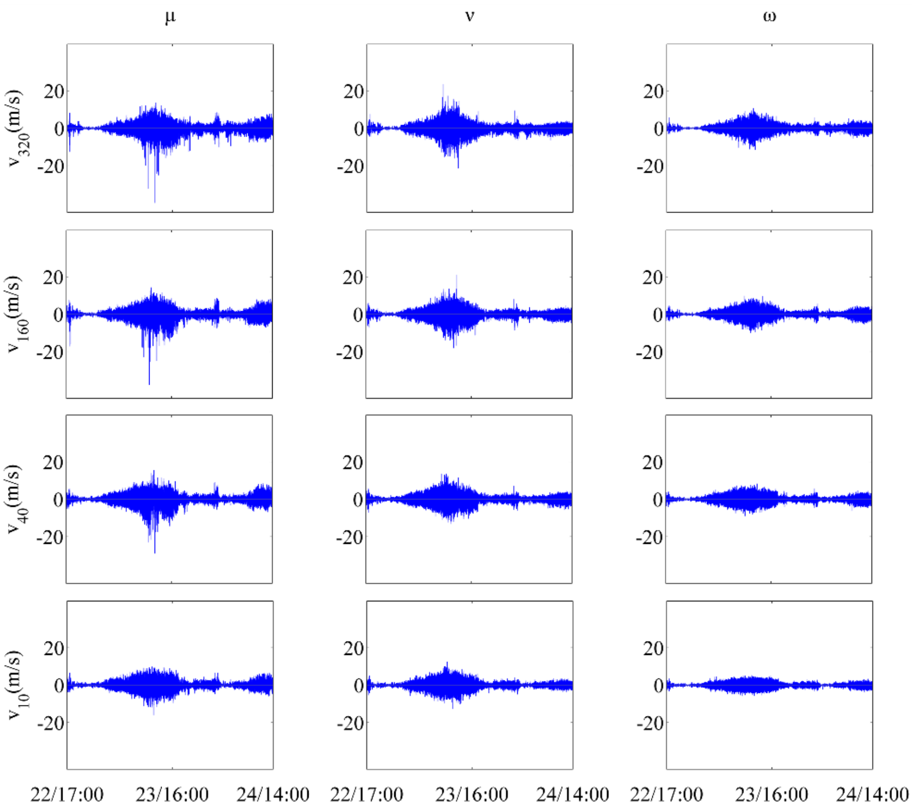

Fig. 7 Time histories of fluctuating wind speeds

3.1.2 Distributions of mean wind speed and direction

Variations of 10-min mean horizontal wind speed and direction are depicted in Fig. 5. The peak value of the 10-min mean horizontal wind speed was 23.5 m/s, and the wind direction mainly varied in the anticlockwise direction from approximately 70° to nearly 290° during the passage of Hato. In addition, the polar distribution and the wind rose diagram of the 10-min mean horizontal wind speed and direction are presented in Fig. 6. The records illustrate that the wind blew mainly from the 30°-90° and 270°-330° sectors, which indicates that the prevailing 10-min mean horizontal wind directions during the typhoon were from the northeast and the northwest. The maximum 10-min mean horizontal wind speed occurred most frequently (15%-20%) within the 300°-330° sector (representing a northwest wind).

3.1.3 Time history of fluctuating wind speeds

Wind velocity is divided into a mean component and a fluctuating component to facilitate the discussion about the wind turbulence characteristics in the following sections. Fig. 7 shows the time histories of the fluctuating wind speeds (in longitudinal-μ, lateral-v and vertical-ω directions) at those four different heights. All the fluctuating components at different heights have consistent variation, and the maximum fluctuating wind speeds in the longitudinal, lateral and vertical directions are approximately 16.2 m/s, 15.6 m/s and 11.7 m/s, respectively.

3.1.4 Wind speed probability distributions

To investigate the wind speed probability distribution function (PDF), both the normal (Norm) distribution function (Melbourne 1977, Li *et al*. 2017) and generalized extreme value (GEV) distribution function (Park and Sohn 2006, He and Li 2014, *et al*. 2018b) are employed to model the wind speeds. The generalized extreme value distribution combines three extreme value distribution into a single form and includes the Gumbel distribution, the Frechet distribution, and the Weibull distribution. The function of the cumulative distribution is:

$$F(xu_g,\sigma_g K)=\exp\left\{-\left[1+K\frac{(x-u_g)}{\sigma_g}\right]^{-\frac{1}{K}}\right\},\qquad 1+K\frac{(x-u_g)}{\sigma_g}>0 \quad (1)$$

where u_g is the location parameter, σ_g is the scale parameter and K is the shape parameter; for $K\rightarrow 0$, $K>0$, $K<0$, the cases correspond to the Gumbel, Fréchet, and Weibull distribution, respectively. Fig. 8 and Fig. 9 show the probability distributions of wind data samples in the x, y and z directions and those of the fluctuating winds in the μ, v and ω directions, respectively. Obviously, the distributions of the selected wind samples in the x, y and z directions could not be fitted well by either the normal distribution function or the generalized extreme value distribution function. However, the wind speeds in the x direction approximately follow the generalized extreme value distribution, as shown in Fig. 8. Meanwhile, the fitting results in Fig. 9 do not show good agreement between the fluctuating winds and the two fitted probability distribution functions.

Obviously, the probability distributions of fluctuating

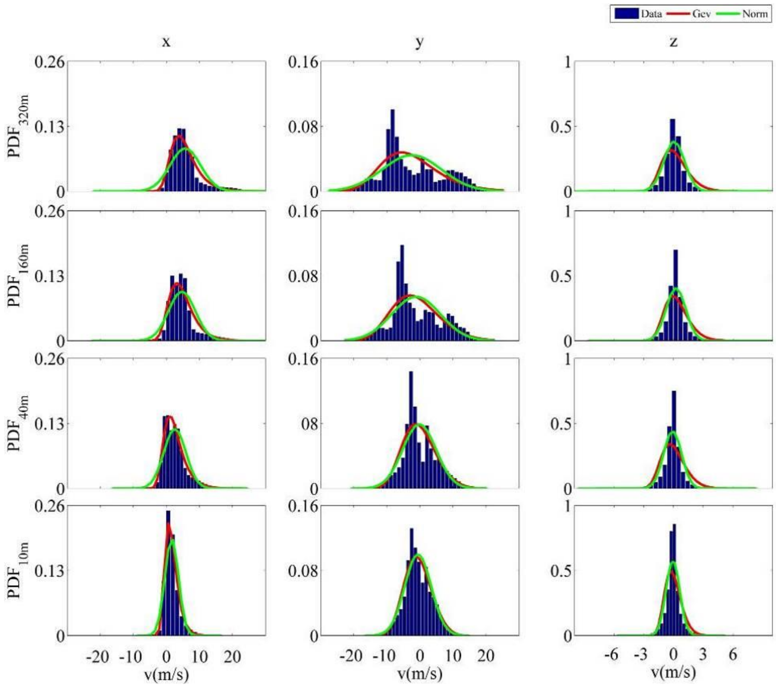

Fig. 8 PDFs of directional wind speeds

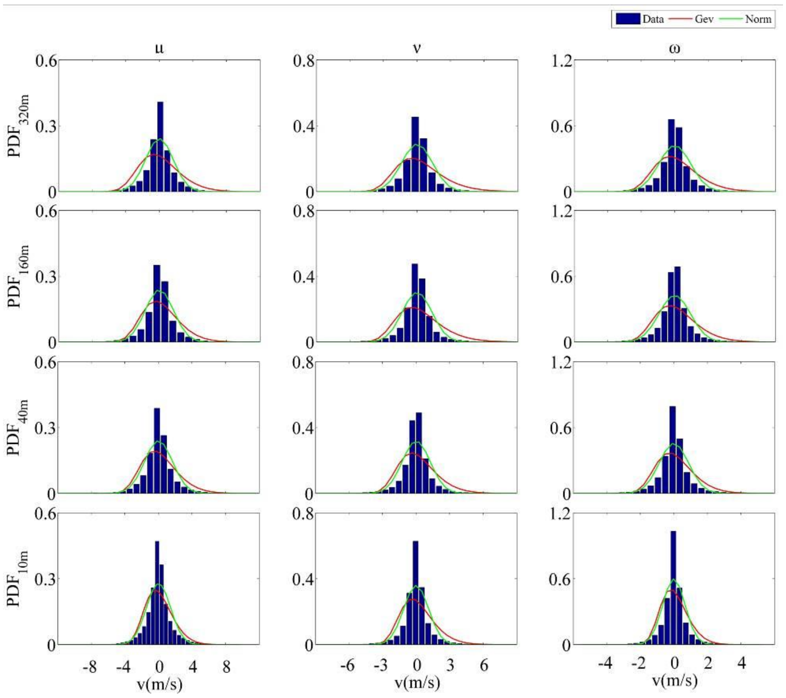

Fig. 9 PDFs of fluctuating wind speeds

winds do not match the normal distribution well over the whole observation period (45 hours). So the probability distribution of a 10-min fluctuating wind segment corresponding to the maximum wind speed period are plotted in Fig. 10, fitted by both the generalized extreme value model and the normal distribution model. The figure shows that the probability distribution of a 10-min fluctuating wind segment follows both the normal distribution and the generalized extreme value distribution very well.

3.2 Gust wind characteristics

3.2.1 Data quality control

This section focuses on analysis of the characteristics of gust wind in terms of energy distribution (spectrum), gust factor and turbulence intensity. As suggested by He *et al*. (2013b), the collected datasets should be checked by a thermally neutral stability test to verify the quality of wind records to be used for further analysis. A neutral stability condition refers to an equilibrium stratification status of air

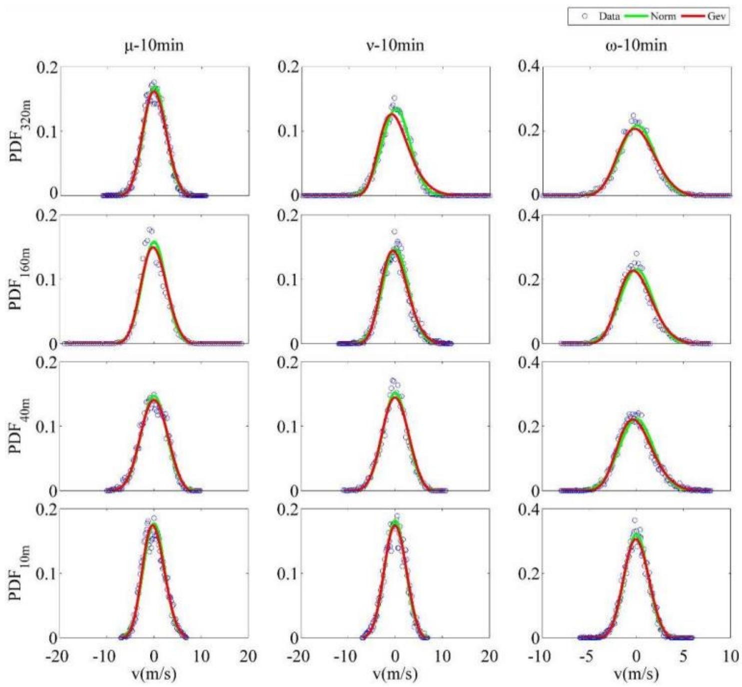

Fig. 10 PDFs of 10-min fluctuating wind speeds

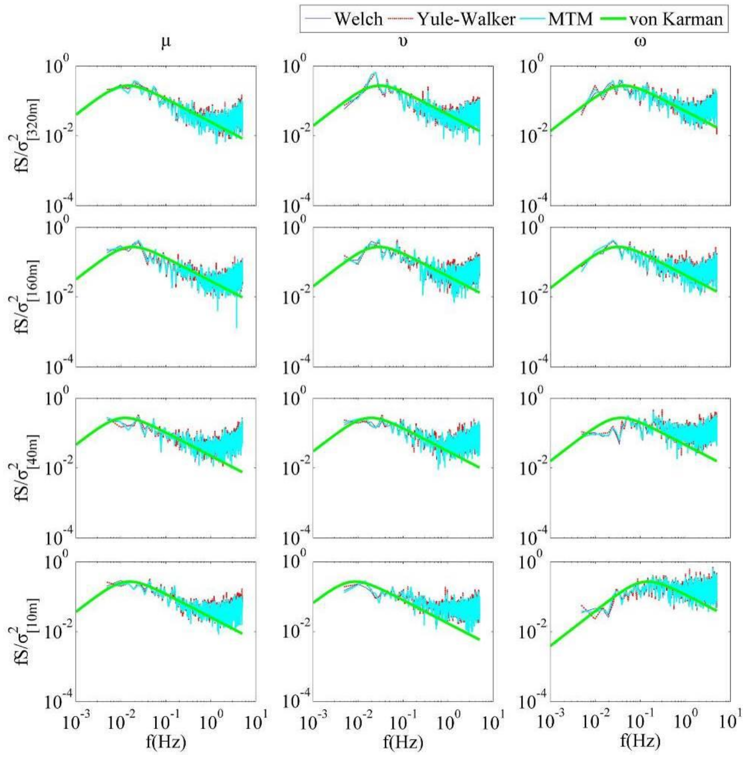

Fig. 11 PSDs of fluctuating wind speeds

flows without typical convection due to a thermal effect. Generally, it can be judged by the Richardson number (Businger *et al*. 1971, Golder 1972, Tieleman 2008) or the ratio of the vertical coordinate to the Obukhov length (Businger *et al*. 1971). In practice, it is suggested that the stability condition can be reasonably assumed if wind speed exceeds a certain value, say 10 m/s, as recommended in the Engineering Science Data Unit (ESDU) (1985). Rolando (2008) recommended 8 m/s as the threshold value beyond which the horizontal flow retardation could be deemed to be unaffected by thermal convection. A smaller value of 5 m/s was adopted in Masters *et al*. (2010) by considering the cloud coverage. He *et al*. (2013b) took values of both 10 m/s and 5 m/s according to different topographical conditions. In this section, the relatively weaker criterion of 5 m/s is adopted for the following analysis of gust winds in

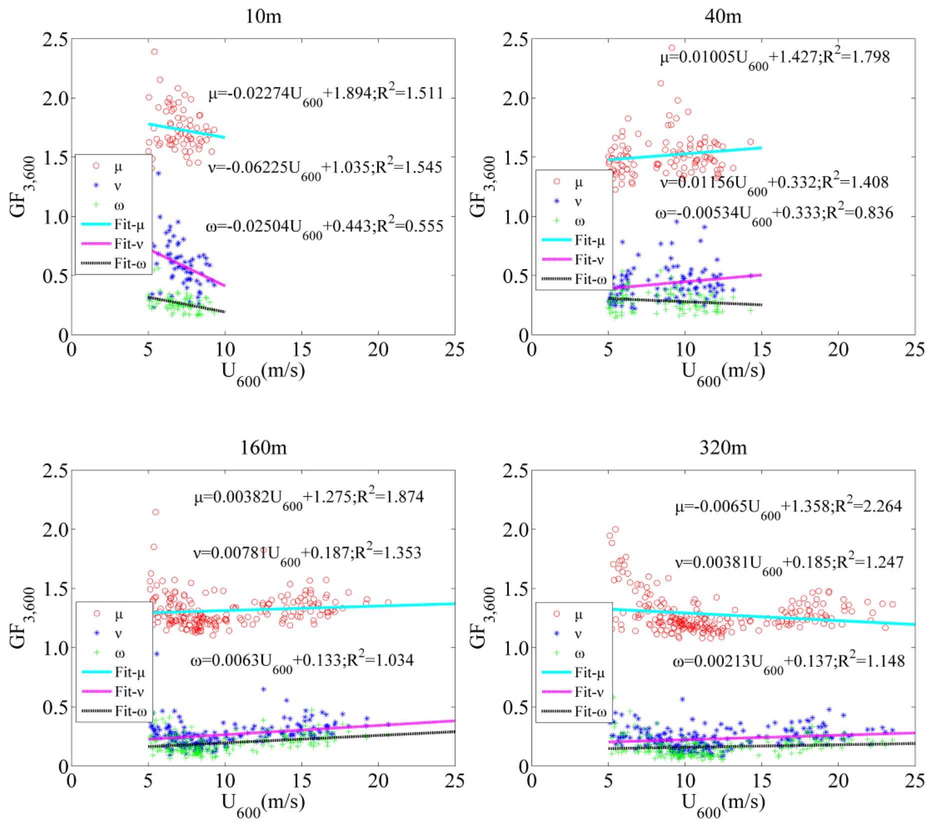

Fig. 12 Gust factors for 3 s wind gusts over a 600 s mean longitudinal wind speed

consideration of the influences due to topographic/terrain obstructions surrounding the observation site (Fig. 1).

3.2.2 Energy distribution

Spectral analysis techniques are widely used to identify the energy distribution of turbulent winds in the frequency domain. Three frequently used methods, i.e., the Welch method (Welch 1967), the multi-taper method (MTM) (He *et al*. 2018a), and the Yule-Walker method (Thomson, 1982), are employed in this study to analyze and discuss the spectral characteristics of the fluctuating winds in different directions. For comparison purposes, a von Karman-type spectral model (Von Karman 1948, Cao *et al*. 2009), which is generally accepted as the best analytical representation of isotropic turbulence (Engineering Science Data Unit (ESDU) 1985), is adopted herein to model each of the fluctuating wind components. Fig. 11 plots the normalized power spectral densities (PSDs) of a selected full 20-min fluctuating wind segment that corresponded to the maximum wind speed period and was associated with the north wind direction (360°). As shown in the figure, the power spectra of fluctuating winds in different directions from the ultrasonic anemometers at the four heights trend similarly within the entire frequency range. Moreover, the wind spectra derived from the above three spectral analysis methods agree well with the von Karman spectrum model within the measured frequency range, especially below 0.1 Hz. However, the wind spectra at the right tail of the frequency range are slightly higher than those of the von Karman spectrum model, which means the wind components from the observations could contain relatively more energy in the higher frequency range than those predicted by the von Karman spectrum model.

3.2.3 Gust factors

Gust factor variations

Numerous field measurement studies have been carried out to investigate the turbulence characteristics of tropical cyclones. However, a review of these studies reveals much inconsistency. Some studies found that gust factors increased slightly with the increase of mean horizontal speeds (Vickery and Skerlj 2005, He *et al*. 2017). Some advocated that gust factors decreased as wind speed increased within a certain range (Ishizaki 1983). Paulsen and Schroeder (2005) showed gust factors were almost independent of mean wind speed. Moreover, Li *et al*. (2009) revealed that the longitudinal gust factor decreased with an increase in mean wind speed, while the lateral and vertical gust factors remained almost unchanged regardless of the variation in the mean wind speed. In addition, capped values were also reported to exist for the cases of very strong winds with speeds over approximately 30 m/s (Powell *et al*. 2003, Vickery *et al*. 2009).

Figs. 12 and 13 present the gust factor values with 3 s and 60 s durations in longitudinal (μ) and lateral (ν) and vertical (ω) directions over 600 *s* mean longitudinal wind speed ($GF_{3,600}$; $GF_{60,600}$), respectively. For each of these figures, gust factors are also fitted using linear regression model. These two figures show that the gust factors are scatted at lower wind speed levels (such as U<10 m/s) and

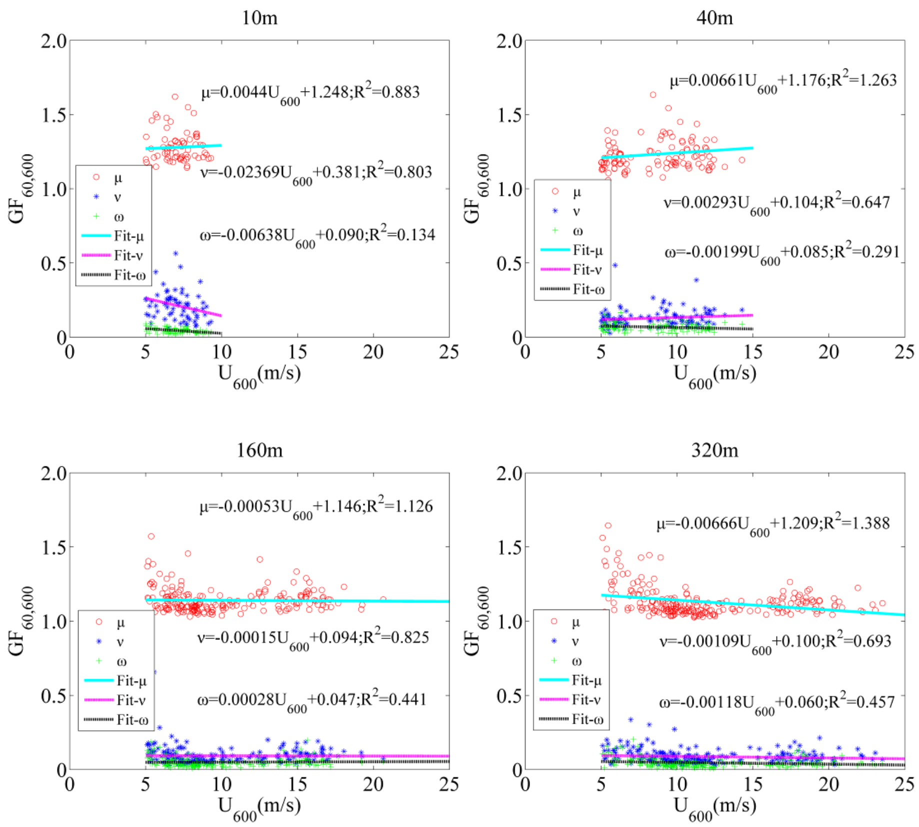

Fig. 13 Gust factors for 60 s wind gusts over a 600 s mean longitudinal wind speed

Table 1 Mean gust factors for fluctuating wind components

Height	U_{600}(m/s)	GF3,600				GF60,600			
		μ	v	ω	*ratio**	μ	v	ω	*ratio**
10 m	7.071	1.733	0.595	0.266	1:0.34:0.15	1.279	0.213	0.045	1:0.17:0.04
40 m	8.597	1.514	0.437	0.287	1:0.29:0.19	1.233	0.129	0.068	1:0.10:0.06
160 m	10.112	1.317	0.266	0.197	1:0.20:0.15	1.141	0.093	0.050	1:0.08:0.04
320 m	11.900	1.281	0.230	0.163	1:0.18:0.13	1.130	0.087	0.046	1:0.08:0.04

*ratio: 'Ratio' denotes GF_μ: GF_v: GF_ω.

are relatively stable in the higher wind speed range. The longitudinal gust factors are much larger than the lateral and vertical gust factors. Specifically, for $GF_{3,600}$, the longitudinal values mainly vary in the range of 1.0 to 2.0, and the values of the lateral and vertical gust factors are between 0 and 1.0. For $GF_{60,600}$, the longitudinal values are mostly within the range of 1.0-1.5, while the lateral and vertical gust factors are concentrated in the range of 0-0.5. Judging from the fitted linear regression models, the change trends of the gust factors with increasing mean wind speeds are inconsistent for different fluctuating components; even between $GF_{3,600}$ and $GF_{60,600}$. In other words, there exist some differences in the variation trends (as shown in Figs. 12 and 13). In addition, the slopes of the fitted lines are small, which means the increasing/decreasing trends in the gust factors are slight. Consequently, it can be concluded from the analyzed results of the observations that the gust factors of fluctuating wind components remain constant with increasing mean wind speed.

The mean values of gust factors and the corresponding mean wind speeds are listed in Table 1, as well as ratios for the gust factor among the three components. Table 1 shows that the ratio of GF_μ:GF_v:GF_ω tends to decrease with increasing height. As expected, the ratio for the $GF_{60,600}$ is obviously smaller than that for the $GF_{3,600}$. In particular, the ratio for $GF_{3,600}$ (1:0.29:0.19) at height of 40 m is very close to the result determined by Li *et al*. (2009) at height of 47 m (1:0.30:0.22).

Gust factors over different time intervals

For comparison convenience, the horizontal gust factors GF_R ($R=\sqrt{\mu'^2+\upsilon'^2}$) for 3 s and 60 s wind gusts over a 600 s duration of mean longitudinal wind speed are presented in Fig. 14. This approach shows the GF_R versus mean wind speed with the data points stratified by the different gust durations. Fine distinctions also exist for the change trends between the $GF_{3,600}$ and $GF_{60,600}$. To further investigate the dependence of the gust factors (*GFs*) on the time intervals, the Durst method (Durst, 1960) is adopted. Herein, the analysis is carried out based on 10-min length segments, i.e., the mean wind duration is T=T_0=600 s while the gust

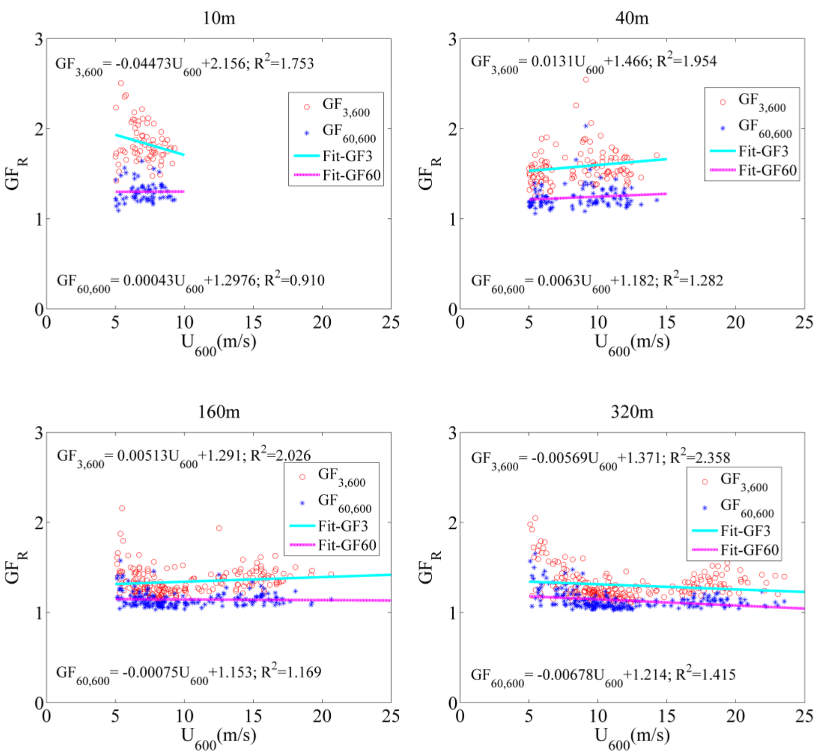

Fig. 14 Comparison of gust factors with 3 s and 60 s wind gusts over a 600 s mean longitudinal wind speed

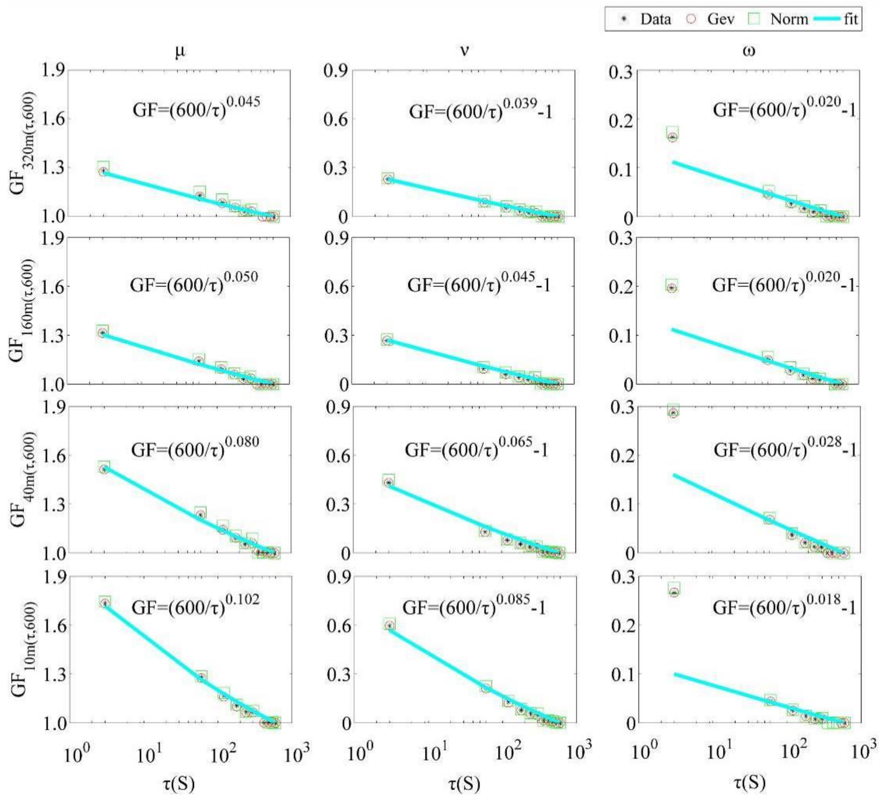

Fig. 15 Gust factor values with respect to varied gust durations

durations τ are 3 s, 1×60 s, 2×60 s, …, 10×60 s. *GFs* with respect to different wind gust durations are depicted in Fig. 16 with a semilog coordinate. Basically, the distributions of the *GFs* are consistent with the results for "at sea" exposure, as summarized in Harper *et al*. (2010), Krayer and Marshall (1992), and Yu and Gan Chowdhury (2009). According to the suggestions given by Harper *et al*. (2010), *GFs* with reference to different gust durations can be fitted with the

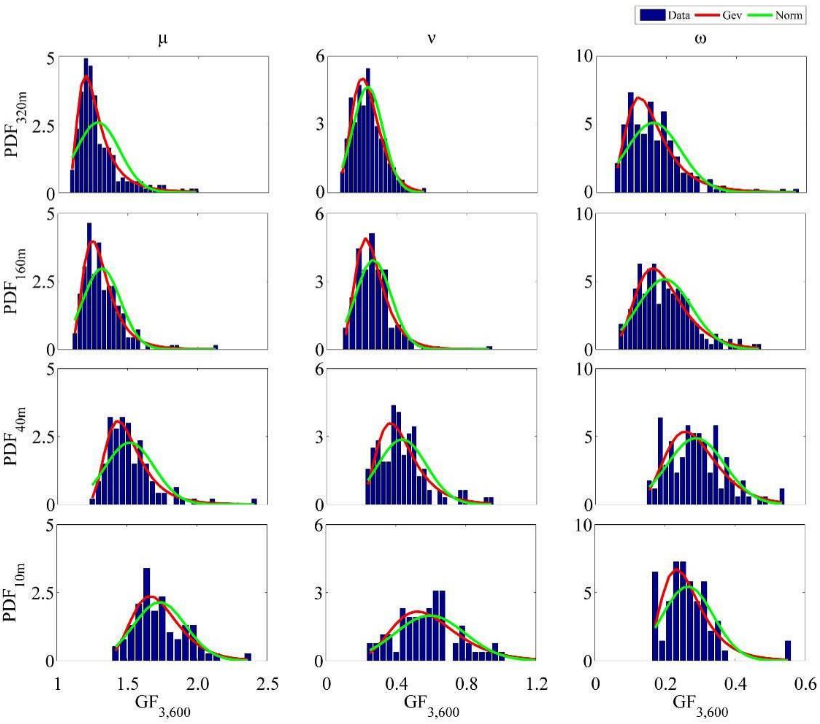

Fig. 16 PDFs of longitudinal, lateral and vertical gust factor values

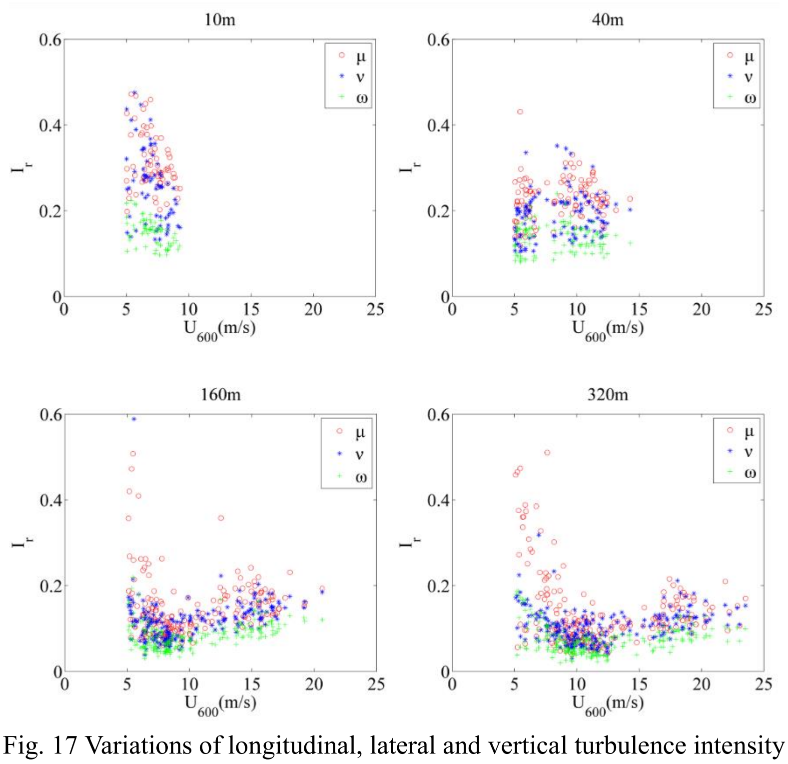

Fig. 17 Variations of longitudinal, lateral and vertical turbulence intensity

following equations:

$$GF_i = (600/\tau)^{a_i},\ i = u \qquad (2)$$

$$GF_i = (600/\tau)^{a_i} \text{-}1,\ i = \nu,\ \omega \qquad (3)$$

where a_i are fitting coefficients. Fig. 15 shows that the fitted curves based on Eqs. (2) and (3) are in good agreement with the distributed *GF* values for the longitudinal and lateral wind components, respectively. However, the proposed expression in Eq. (3) fails to make an appropriate fit for the vertical component.

PDF of Gust factors

As shown in Fig. 15, the GF values are also fitted by

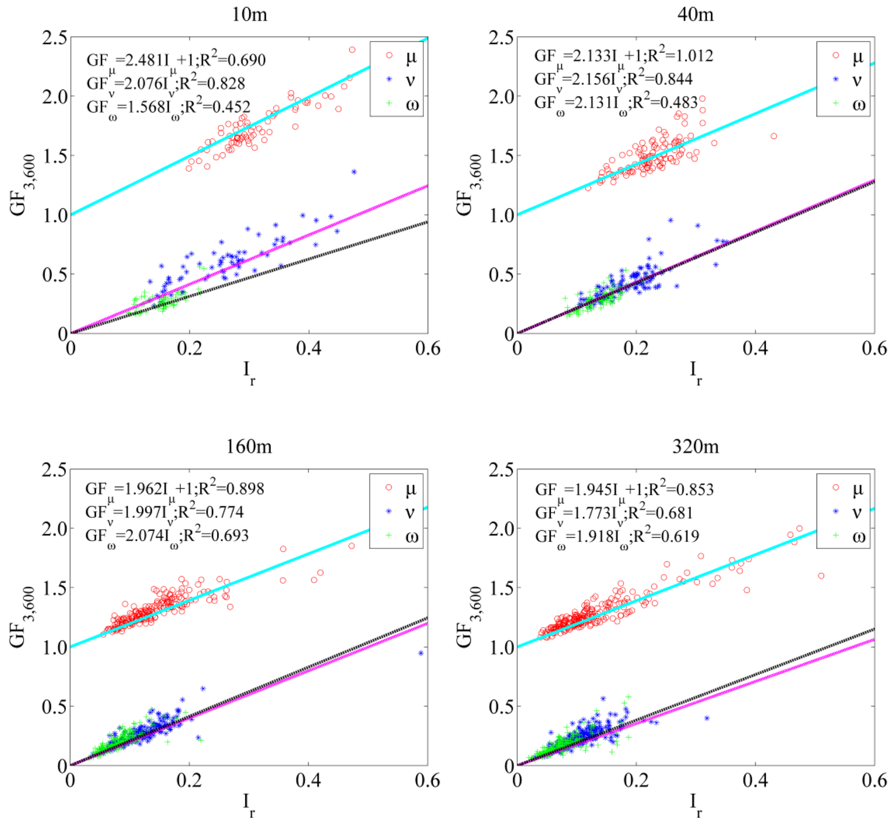

Fig. 18 Correlations between the gust factor and turbulence intensity in longitudinal, lateral and vertical directions

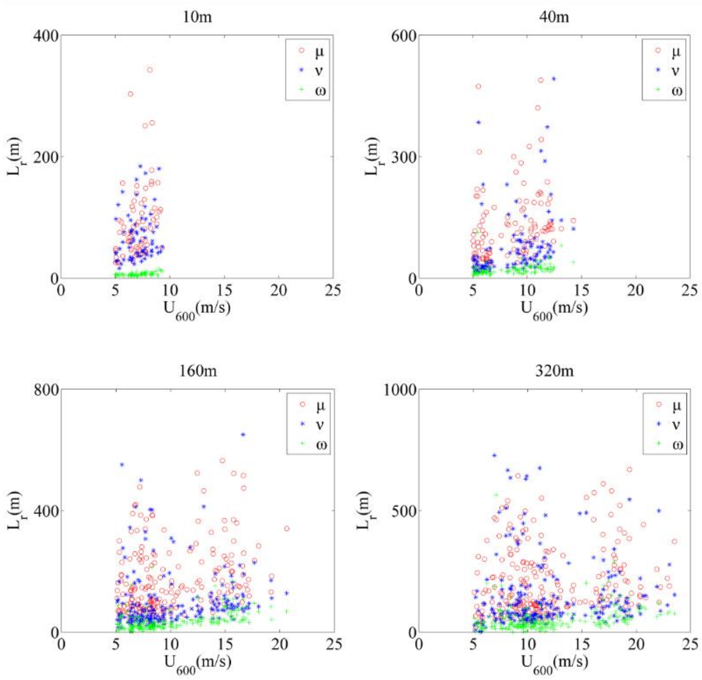

Fig. 19 Values of longitudinal, lateral and vertical turbulence integral length scales

both the generalized extreme value model and the normal distribution model. The *GF* values seem to be close to the two models. To further examine the degree of closeness, the probability distribution of $GF_{3,600}$ for a 3 s wind gust is presented in Fig. 16. The obtained $GF_{3,600}$ values follow the GEV distribution well. By contrast, the normal distribution provides a less similar description. It is interesting to note that although the probability distribution of fluctuating winds over the whole observation period (45 hours) is not fitted well by either the GEV or the Normal distributions (as shown in Fig. 9), the probability distributions of the gust factors can still be described approximately using the

Table 2 Averaged turbulence intensity and turbulence integral length scales

Height	U_{600}(m/s)	*I*				*L*			
		μ	*v*	*ω*	*ratio**	*μ*	*v*	*ω*	*ratio**
10 m	7.071	0.311	0.258	0.150	1:0.83:0.48	92.74	67.66	6.63	1:0.73:0.07
40 m	8.597	0.236	0.190	0.136	1:0.81:0.58	148.81	76.12	21.98	1:0.51:0.15
160 m	10.112	0.145	0.118	0.083	1:0.81:0.57	174.27	100.40	36.69	1:0.58:0.21
320 m	11.900	0.133	0.105	0.073	1:0.79:0.55	212.85	146.67	52.53	1:0.69:0.25

*ratio: 'Ratio' denotes the I_μ:I_v:I_ω or L_μ:L_v:L_ω

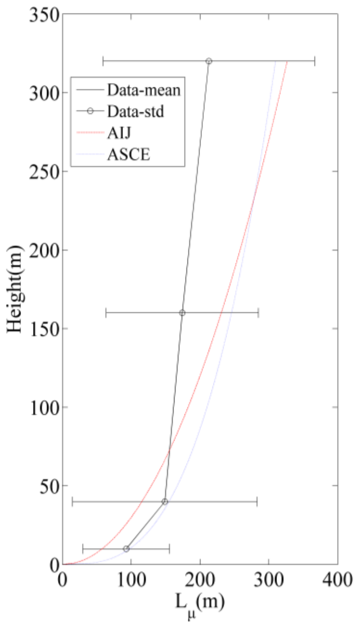

Fig. 20 Vertical profile of longitudinal turbulence integral length scale

generalized extreme value model.

3.2.4 Turbulence intensity

Turbulence intensity variation

Turbulence intensity (I) is an important parameter in wind engineering applications. The statistical results of previous studies show that there tends to be higher values of turbulence intensity for lower mean wind speeds (say, U from 5 to 10 m/s) due to the influence of instability in the lower wind speed range. (Ishizika 1983, Li *et al*. 2009, Peng *et al*. 2018). Fig. 17 shows the turbulence intensity values of the three components of fluctuating wind speeds (denoted as Ir, the subscript r refers to μ, ν or ω) at the four heights. The values are widely scattered when the mean wind speed is lower than 10 m/s. Additionally, the turbulence intensity values for the longitudinal and lateral components are similar and fluctuate mainly within the range of 0.1 to 0.4, which are close to the statistical results derived from field measurements during four typhoons and three hurricanes (Li *et al*. 2019), while the turbulence intensity for the vertical component is distinctly smaller, fluctuating between 0 and 0.2.

Correlations between gust factor and turbulence intensity

Fig. 18 shows the correlations between the gust factor (GF) and turbulence intensity (I) for each component of fluctuating wind speeds. The model described by Ishizika (1983) or an updated form introduced by Cao *et al*. (2009) is adopted to fit the correlations for the longitudinal, lateral and vertical wind components:

$$GF_i(\tau,T)=1+k_1\times I^{k_2}\times\ln(T/\tau),\ i=u \tag{4a}$$

$$GF_i(\tau,T)=k_1\times I^{k_2}\times\ln(T/\tau),\ i=v,\ \omega \tag{4b}$$

where k_1 and k_2 are fitting coefficients. Herein, k_2 = 1. The well-fitted results indicate that the correlations of the GF and I have linear forms as shown in Fig.18.

Turbulence integral length scale

The turbulence integral length scale assigns a spatial dimension to the turbulence structure of wind flows, which is identified as the average eddy size. In this paper, the turbulence integral length scale (L_i) is calculated by the following equation (Flay and Stevenson 1988):

$$L_i=\frac{U}{\sigma_i}\int_0^\infty R(\tau)d\tau,\ (i=\mu,\ \upsilon,\ \omega) \tag{5}$$

where U is the mean wind speed, σ is the standard deviation, and $R(\tau)$ is the autocorrelation function of the fluctuating wind speeds.

Fig. 19 shows variations of the three-dimensional turbulence integral length scales with the longitudinal mean wind speed measured at the four heights during Typhoon Hato. Similar to the turbulence intensity, the longitudinal and lateral turbulence integral length scales are close to each other, while the values of the vertical length scale are much smaller. In addition, the figure also shows that the turbulence integral length scales tend to be larger for higher wind strength, i.e., there is an increasing trend for all the three-dimensional turbulence integral length scales with increasing mean wind speed.

Table 2 lists the averaged turbulence intensity and turbulence integral length scales measured at the four heights, along with their ratios in the three directions. Particularly, the average values of longitudinal turbulence integral length scale are close to those measured from other typhoons and hurricanes (Li *et al*. 2019). In addition, the ratios for turbulence intensity for different height levels are very similar, while the ratios for turbulence integral length scales show some differences. The obtained I_μ:I_v:I_ω values from the field measurements at the four heights during the typhoon are consistent with that (I_μ:I_v:I_ω= 1: 0.75: 0.50) suggested by Solari and Piccardo (2001), and the ratio of

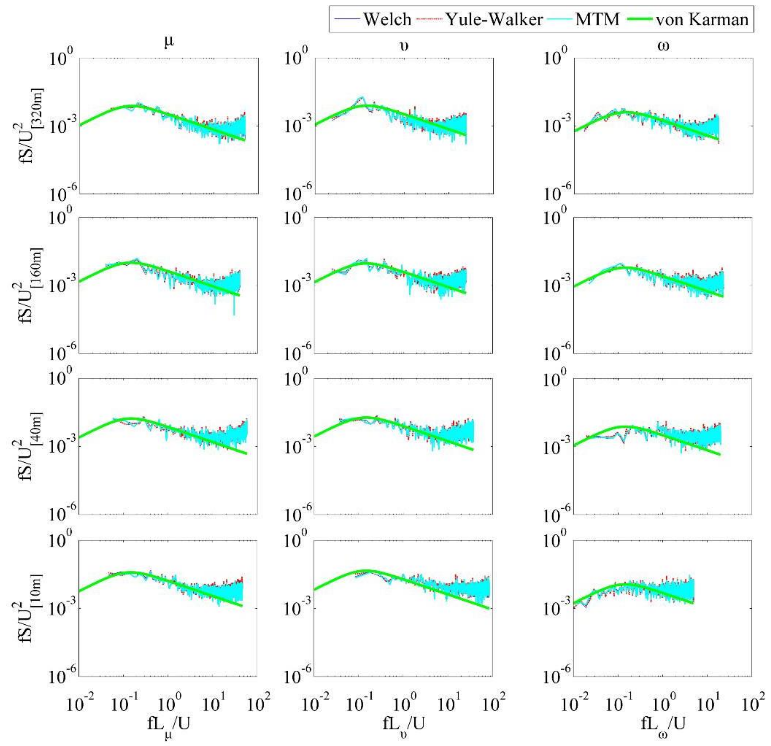

Fig. 21 Jointly normalized spectra with turbulence integral length scale

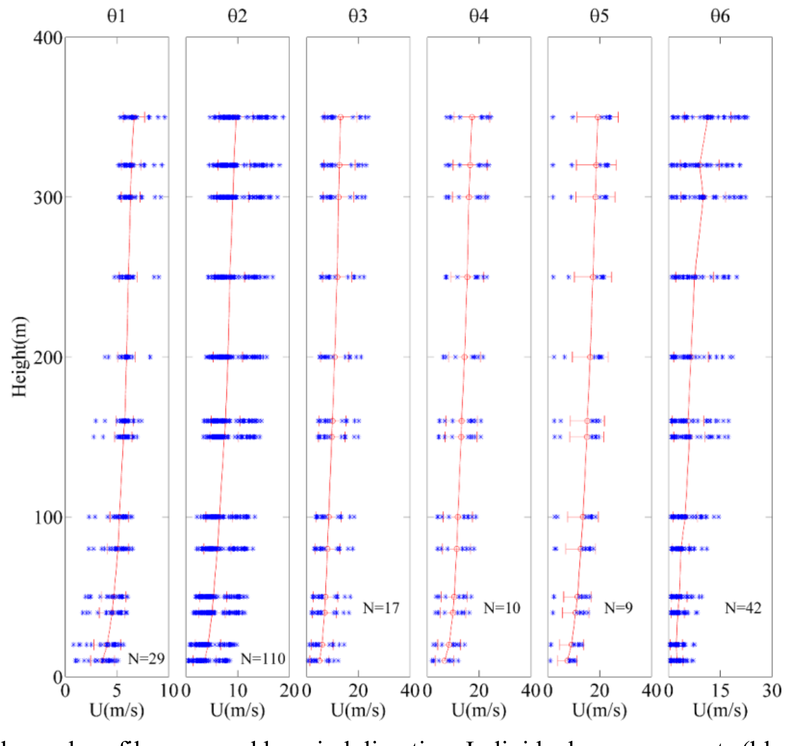

Fig. 22 10-min mean wind speed profiles grouped by wind direction. Individual measurements (blue dots), mean (red circles), standard deviation (red horizontal bars), fitting line (red line), and N (number of qualified profiles)

L_μ:L_ν:L_ω at the height of 40 m (1:0.51:0.15) is also close to the result presented by Li *et al*. (2009) at a height of 47 m (1:0.50:0.16). The profile of the measured longitudinal turbulence integral length scales is plotted in Fig. 20 which also displays the profiles determined by empirical formulas recommended by AIJ-RLB-1996 (1996) and ASCE (1998):

$$L_\mu = 100(z/30)^{0.5} \qquad \text{(AIJ-RLB-1996)} \tag{6}$$

$$L_\mu = l(z/10)^{\varepsilon} \qquad \text{(ASCE)} \tag{7}$$

where l and ε are terrain-related parameters; herein, l= 100 and ε=1/3.

For heights of 10 m, 40 m and 160 m, the predicted values are relatively close to the measured ones, while a larger difference exists for the 320 m height, implying that these two empirical models can be used for prediction of longitudinal turbulence integral length scales at relatively low heights.

Normalized spectra with turbulence integral length scale

As described in Section 3.2.2, the normalized power spectral densities of a selected wind segment are illustrated in Fig. 11. According to the obtained turbulence integral length scale, the frequency range can also be normalized with the ratio of turbulence integral length scale to mean wind speed (L/U). Fig. 21 presents the jointly normalized (both power and frequency) spectra results with the turbulence integral length scale and mean wind speed. The derived spectra results are consistent with those in Fig. 11 in terms of the energy distribution and change trend of the spectral curves. Moreover, the close agreement between the wind measurement spectral analysis results and the prediction of the von Karman spectrum equation demonstrates the accuracy and reliability of the spectrum estimation method for determining the turbulence integral length scale based on the von Karman spectrum model (He *et al*. 2013b).

3.3 Wind profiles

3.3.1 Measured wind speed profiles

As mentioned in Section 3, the wind measurements from both cup anemometers/wind vanes and ultrasonic anemometers installed at 13 heights on the SMT can be used to determine the vertical wind profiles during the passage of typhoon Hato.

Considering the topography features among different azimuths surrounding the observation site, the wind profiles are determined in a composite sense, grouped by wind direction. As shown in Fig. 6, the prevailing 10-min mean wind directions during the typhoon were from the northeast and northwest. So the selected profiles were grouped into 6 sectors for display according to wind directions, from 270° clockwise to 90° (i.e., θ1=270° to 300°; θ2=300° to 330°; θ3=330° to 360°; θ4=0° to 30°; θ5=30° to 60°; θ6=60° to 90°). The composite wind profiles corresponding to each sector are collectively given in Fig. 22. The results indicate that the composite wind profiles generated from the measurements do not show marked differences between sectors. All the composite wind profiles show a gradual increase from 10 to 350 m, except for θ6 (east wind), which has a slight fluctuation along the tower height, which can be attributed to the topographic effects on the wind speed measurements in these sectors, e.g., possibly to the obstruction caused by the hilly terrain in the corresponding upwind directions as shown in Fig. 1.

Strong winds are usually regarded as being in a thermally neutral condition (Tse *et al*. 2013, Tamura 2015, He *et al*. 2016). Therefore, in order to investigate the influence of wind speed on the measured wind profiles, Figure 23 show the composite wind profiles grouped by wind speed on the basis of 10-min mean wind speed at the 40 m height (i.e., U (40) ∊ (0, 5]; U (40) ∊ (5, 10]; U (40) ∊ (10, 15]; U (40) ∊ (15, 20]), as well as the wind speed normalized by U (40). Additionally, all the composite wind speeds increase slightly over the entire height and show similar wind profile shapes. However, in the case of U (40) ∊ (0, 5], there are some "kinks" along the entire height, implying that lower wind speeds were likely associated with a nonstationary state due to thermal effects.

3.3.2 Empirical models of wind speed profile

For comparison purposes, frequently used empirical models, including the log law (Kustas and Brutsaert 1986, Zilitinkevich *et al*. 2008), the power law (Davenport 1960) and the Deaves-Harris (D-H) model (Deaves 1981, Tieleman 2008), are adopted in this section to fit the vertical distribution of mean wind speed during Typhoon Hato:

$$U(z)=\left(\frac{U_o^*}{\kappa}\right)\ln\left(\frac{z-z_d}{z_0}\right) \tag{8}$$

(Log law)

$$\frac{U(z)}{U(z_{ref})}=\left(\frac{z}{z_{ref}}\right)^{\alpha} \tag{9}$$

(Power law)

$$\frac{U(z)}{U_0^*}=\frac{1}{\kappa}\left\{\ln\left(\frac{z}{z_0}\right)+5.75\frac{z}{h}-1.88\left(\frac{z}{h}\right)^2-1.33\left(\frac{z}{h}\right)^3+0.25\left(\frac{z}{h}\right)^4\right\} \tag{10}$$

in which $h=\dfrac{U_0^*}{Bf}$

(D-H model)

where $U(z)$ is the mean wind speed at height z; U_0* is the surface friction velocity, which can be obtained based on measured fluctuating winds ($U_0^*=\left(\overline{-\mu\omega}\right)^{1/2}$, overbar represents the mean); κ is von Karman's constant (here κ=0.4); z_d is the zero-plane displacement; z_0 is the surface roughness length; $U_{(zref)}$ is the mean wind speed at the reference height z_{ref}; α is the ground roughness exponent; the magnitude of B based on observed wind profiles is 6; and f is the Coriolis parameter (here f=9.375×10-5 s^{-1} with latitude about 40°).

3.3.3 Estimation of atmospheric stability

For comparison with the empirical models of wind speed profile, it is necessary to eliminate the influence of thermal instability on the measured wind profiles. Herein, both the ratio of the height z to the Obukhov scaling length (z/L) and the Richardson number (Ri) are adopted to evaluate the air flow stability (Businger *et al*. 1971, Tieleman 2008, Golder 1972):

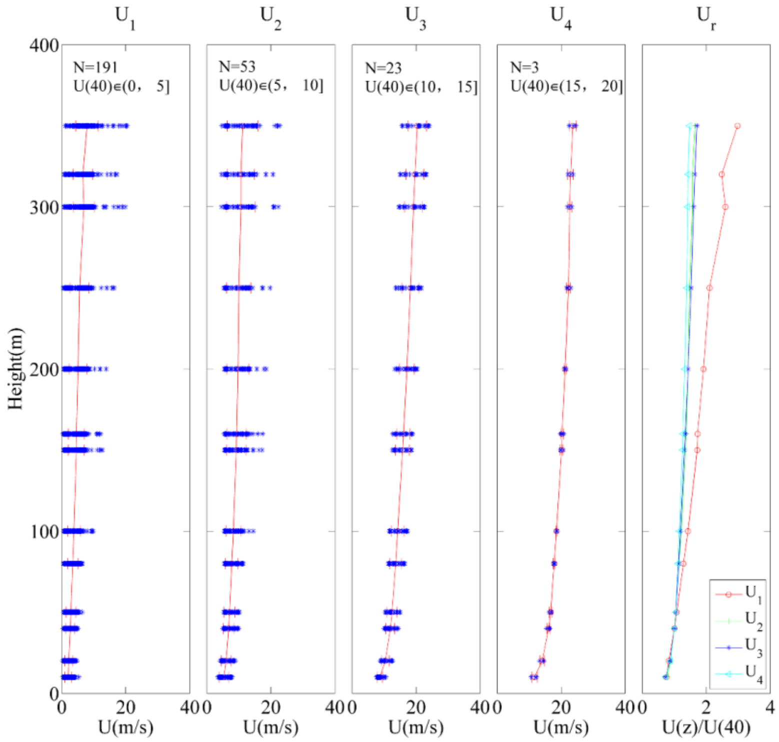

Fig. 23 10-min mean wind speed profiles grouped by wind speed. Individual measurements (blue dots), mean (red circles), standard deviation (red horizontal bars), fitting line (red line) and N (number of qualified profiles)

$$\frac{z}{L}=-\frac{z\kappa g\overline{\omega'\theta'}}{\bar{\theta}\left(U_0^*\right)^3} \tag{11}$$

$$Ri=-\frac{g\,\partial\bar{\theta}/\partial z}{\bar{\theta}\left(\partial\bar{U}/\partial z\right)^2} \tag{12}$$

where κ is von Karman's constant (0.4), g is the acceleration of gravity, $\overline{\omega'\theta'}$ is the surface heat flux, $\bar{\theta}$ is the mean potential temperature, U_0* is the surface friction velocity, and $\bar{U}$ is the mean wind speed.

In general, values of *z/L* equal to or near zero could be considered to indicate that the wind flow is near-neutral or neutral. According to Li *et al*. (2009), a range of *z/L* within [-0.05, 0.05] was considered herein as a near-neutral air flow. Fig. 24 presents variations of the *z/L* values from the ultrasonic anemometers at 10 m, 40 m, 160 m and 320 m in height, in which the semilogarithmic coordinate form is used to illustrate those values more clearly. At heights of 10 m and 40 m, there are a relatively larger number of values of *z/L* (mainly during the period from 04:00 to 24:00 on August 23) within the range of -0.05 to 0.05, while those for heights of 160 m and 320 m are much smaller. The Richardson numbers for different levels are depicted in Fig. 25 on a semilog coordinate. For comparison purposes, four specific layers, i.e., 10-40 m (layer 1), 10-80 m (layer 2), 10-100 m (layer 3) and 10-160 m (layer 4) are selected to examine the distribution of *Ri* values. In particular, based on the discussion and suggestion for the stability parameter value range from previous studies (Businger *et al*. 1971, Golder 1972, Good 2012), for a neutral condition, the upper and lower limits of the *Ri* number are recommended to be 0.2 and -0.1, respectively. Fig. 25 shows that for layer 1, *Ri* values within the range of [-0.1, 0.2] were mainly found between 10:00 and 24:00 on August 23, while that range of values for layer 2 mainly occurred approximately 12:00 on August 23. By contrast, there are very few *Ri* values within the range of -0.1 to 0.2 for both layer 3 and layer 4.

The distributions of *z/L* values and *Ri* values indicate that the neutral condition profiles were mainly from 04:00 to 24:00 on August 23, with wind flows below 80 m in heights. Consequently, only the datasets of the 10-min mean wind speed at heights of 10 m, 20 m, 40 m, 50 m and 80 m under neutral conditions are selected, and the averaged results of those qualified samples are adopted for the following wind profile examination.

3.3.4 Evaluation of roughness length and zero-plane displacement

As shown in Eqs. (8) - (10), the roughness length (z_0) and zero-plane displacement (z_d) are two essential parameters in the empirical models. In this paper, the two most common methods, the Lettau wind profile method (Lettau 1957, Grimmond 1998) and the extension of mass conservation method (EMCM) (De Bruin and Moore 1985, Lacy 2011), are chosen to determine z_0 and z_d based on the measured wind profiles under neutral conditions. The Lettau method is an iterative process to determine the zero-point displacement D (D=z_0-z_d) for the condition of the minimized sum of the squared error:

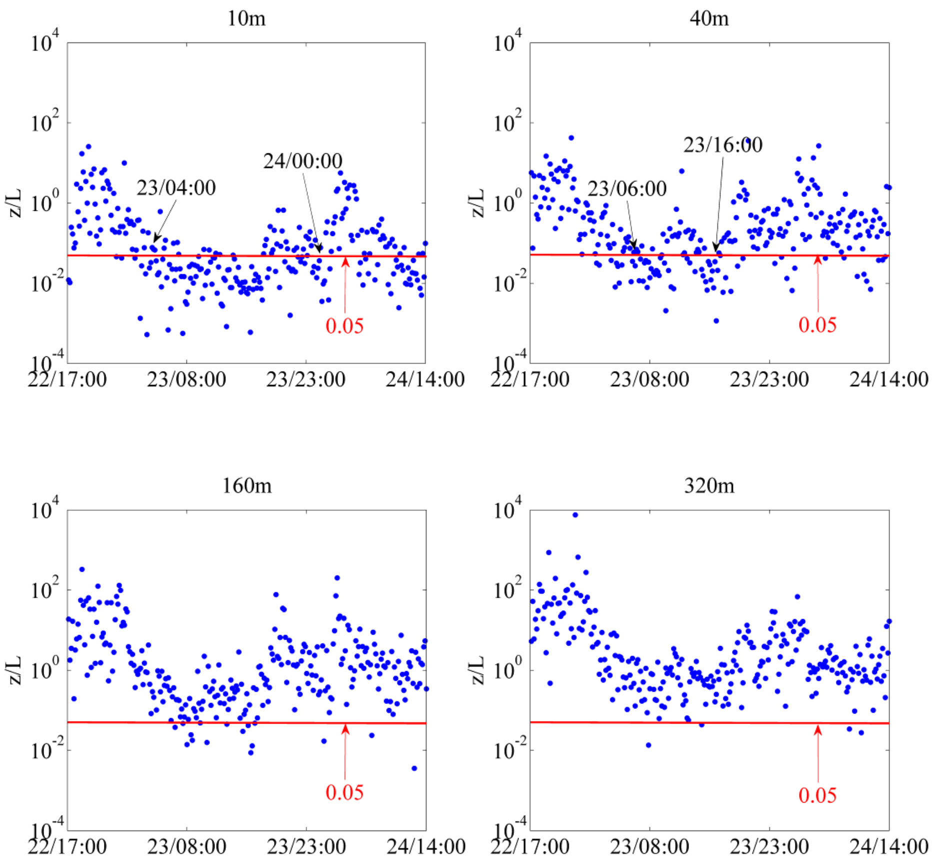

Fig. 24 Variation of the z/L values at four height levels

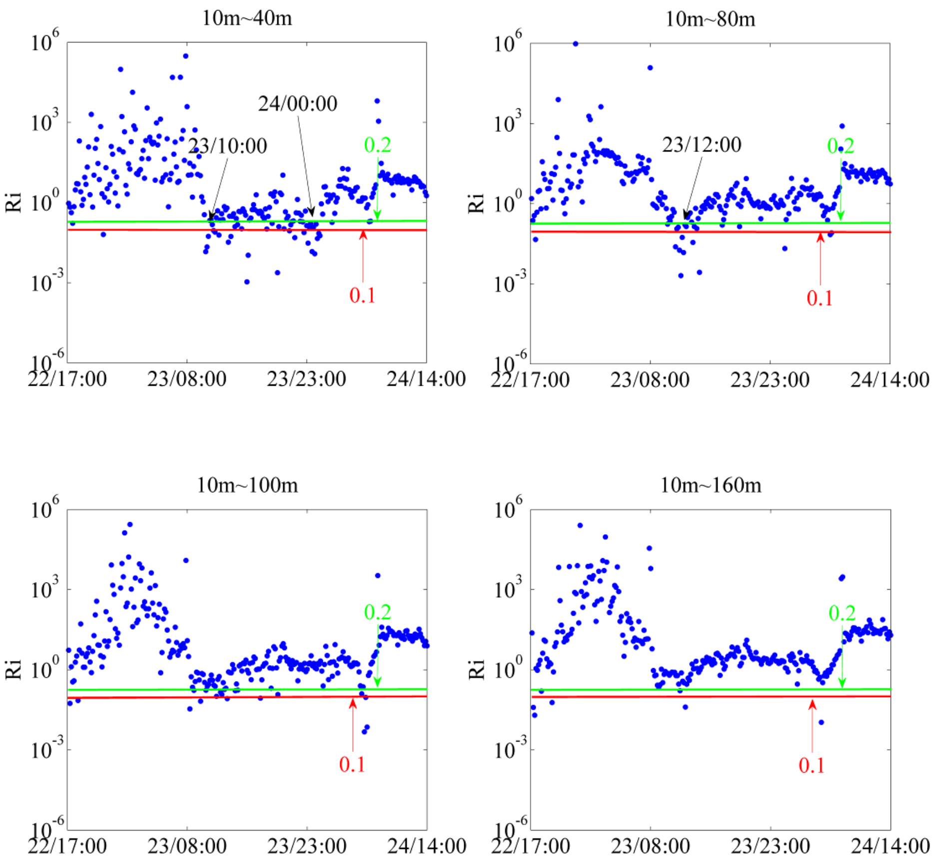

Fig. 25 Variation of the Ri values between different levels

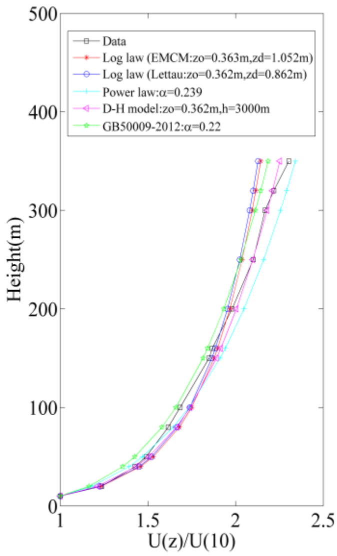

Fig. 26 Comparison of the measured 10-min mean speed profile with those fitted by the empirical models

$$\sum_{i=1}^{N}\varepsilon^2=\sum_{i=1}^{N}\left[\left(U_i-\overline{U_N}\right)-\frac{U_0^*}{\kappa}\left(\ln\left(z_{si}+D\right)-\overline{\ln\left(z_{si}+D\right)}\right)\right]^2 \tag{13a}$$

$$\frac{U_0^*}{\kappa}=\frac{\sum_{i=1}^{N}\left[U_i-\overline{U_N}\right]\left[\ln\left(z_{si}+D\right)-\overline{\ln\left(z_{si}+D\right)}\right]}{\sum_{i=1}^{N}\left[\ln\left(z_{si}+D\right)-\overline{\ln\left(z_{si}+D\right)}\right]^2} \tag{13b}$$

where U_i is the mean wind speed at a level z_{si} of those selected N levels, U_0* is the surface friction velocity, κ is von Karman's constant (here κ=0.4) and the overbar indicates the mean of the N levels. When D and U_0* are determined, z_0 and z_d can be obtained with wind speed at one level as follows:

$$z_0=\left(z_s+D\right)\exp\left(-\frac{U_z\kappa}{U_0^*}\right) \tag{13c}$$

$$z_d=z_0-D \tag{13d}$$

In the extension of mass conservation method, the basic assumption is that the mass transport in the actual profile is equal to that in the theoretical displaced logarithmic profile below an elevation z_f and within the inertial sublayer (De Bruin and Moore 1985):

$$\int_0^{z_f}U\left(z\right)dz=\int_{d+z_0}^{z_f}\frac{U_0^*}{\kappa}\ln\left\{\frac{z-z_d}{z_0}\right\}dz \tag{14}$$

Eq. (14) can be reduced to

$$z_d=z_f-\frac{z_f-\left(z_d+z_0\right)}{\ln\left[\frac{z_f-z_d}{z_0}\right]}-z_m \tag{15a}$$

with the term z_m, given by

$$z_m=\int_0^{z_f}\frac{U(z)}{U\left(z_f\right)}dz=\frac{1}{2U\left(z_f\right)}\left[\sum_{i=2}^{N}\left(U_i+U_{i-1}\right)\left(z_i-z_{i-1}\right)+U_1z_1\right] \tag{15b}$$

Based on obtained U_0*, the z_d and z_0 can be determined as follows

$$z_d=z_f-\frac{z_m}{A};\quad z_0=\frac{z_m}{A}e^{-y_f} \tag{15c}$$

In which

$$y_f=\ln\left[\frac{z_f-z_d}{z_0}\right]=\frac{\kappa U\left(z_f\right)}{U_0^*};\quad A=1-\frac{1-e^{-y_f}}{y_f}$$

where z_f represents a level within the inertial sublayer, and other quantities have been previously defined.

The measured profiles and the fitted results from the empirical models with derived parameters (z_0 and z_d) from the above two methods are illustrated in Fig. 26, which are normalized with the wind speed at 10 m height (U (10)). In addition, the empirical mean speed profile (power-law form) based on the parameters stipulated in the Chinese National Load Code (GB50009-2012) are also presented in Fig. 26. There are no marked differences observed between the measured wind profile and the empirical profiles.

Specifically, the measured mean wind speed profile agrees admirably with that determined by the D-H model. The profiles of the Log-law models (with z_0 and z_d derived from both the Lettau method and the extension of mass conservation method) and power-law models (with α derived from both measured data and the Chinese National Load Code) are also well fitted to the measured data below approximately 200 m. However, at higher elevations (above 200 m), there are relatively large differences between the predicted and the measured results. In general, the empirical models can provide reasonable predictions for the measured wind speed profiles.

5. Conclusions

Based on the field measurements collected from the Shenzhen Meteorological Tower during severe Typhoon Hato, this paper investigated the typhoon-generated wind characteristics in the ABL, including wind spectrum, gust factor, turbulence intensity and length scale as well as wind profile, over a coastal urban area. The main findings and conclusions are summarized as follows

- For a relatively longer data segment of fluctuating wind speeds, the probability distributions were not fitted well by either a normal distribution or a generalized extreme value distribution. In contrast, the probability distribution of 10-min fluctuating winds followed both the normal distribution and the generalized extreme value distribution very well.\

• The normalized power spectra of measured fluctuating winds in different directions from ultrasonic anemometers at four heights have similar trends and also agree well with the von Karman spectral model within the measured frequency range. Furthermore, according to the obtained turbulence integral length scale, the frequency range can be normalized with the ratio of turbulence integral length scale to mean wind speed. The close agreement between the jointly normalized spectra of the wind measurements and the predictions of the von Karman spectral model demonstrates the accuracy and reliability of the spectral estimation method for determining the turbulence integral length scale of winds based on the von Karman spectral model.

• Gust factors of fluctuating wind components remained almost unchanged with increasing mean wind speed. Empirical formulas for gust factor with respect to different wind gust durations were proposed. The probability distribution of gust factors can be approximately described using the generalized extreme value model.

• The relationship between gust factor (GF) and turbulence intensity (I) of the three components of fluctuating wind velocity can be depicted by linear models. For both turbulence intensity and turbulence integral length scales, the longitudinal and lateral items were similar, while the vertical components were much smaller. There was an increasing trend for the turbulence integral length scale with increasing mean wind speed. Additionally, the observational results showed that the empirical models recommended by AIJ and ASCE can be used for prediction of longitudinal turbulence integral length scales at relatively low elevations.

• The influences of the topography features and wind speeds on the wind profiles were investigated based on the field-measured wind records. The vertical wind profiles tended to exhibit some "kinks" for the cases of hilly terrain in the upwind directions or lower wind speeds, which may be attributed to the effects of thermally nonstationary conditions. In addition, the qualified wind profile segments under neutral conditions were selected and averaged to compare with the empirical models of wind speed profile. In general, the empirical models can provide reasonable predictions for the measured wind speed profiles.

Acknowledgments

The work described by this study was fully supported by a grant from the National Natural Science Foundation of China (Project No: 51978593), a grant from the Research Grants Council of Hong Kong Special Administrative Region, China (Project No: CityU 11207519) and a grant from the Research Committee of City University of Hong Kong (Project No: 7005037).

References

AIJ-RLB-1996 (1996), "AIJ recommendations for loads on buildings", Architectural Institute of Japan; Tokyo, Japan.

Amano, T., Fukushima, H., Ohkuma, T., Kawaguchi, A. and Goto, S. (1999), "The observation of typhoon winds in Okinawa by Doppler sodar", *J. Wind Eng. Ind. Aerod.*, **83**(1-3), 11-20. https://doi.org/10.1016/S0167-6105(99)00057-4.

ASCE 7-98 (1998), "Minimum design loads for buildings and other structures", Amer. Soc. Civil Eng., U.S.A.

Bouffard, F. and Galiana F.D. (2008), "Stochastic security for operations planning with significant wind power generation", *In 2008 IEEE Power and Energy Society General Meeting-Conversion and Delivery of Electrical Energy in the 21st Century* IEEE.

Businger, J.A., Wyngaard, J.C., Izumi, Y. and Bradley, E.F. (1971), "Flux-profile relationships in the atmospheric surface layer", *J. Atmos. Sci.*, **28**(2), 181-189. https://doi.org/10.1175/1520-0469(1971)028<0181:FPRITA>2.0.CO;2.

Cao, S., Tamura, Y., Kikuchi, N., Saito, M., Nakayama, I. and Matsuzaki, Y. (2009), "Wind characteristics of a strong typhoon", *J. Wind Eng. Ind. Aerod.*, **97**(1), 11-21. https://doi.org/10.1016/j.jweia.2008.10.002.

Davenport, A.G. (1960), "Rationale for determining design wind velocities", National Research Council of CANADA OTTAWA Div of Building Research.

De Bruin, H.A.R. and Moore, C.J. (1985), "Zero-plane displacement and roughness length for tall vegetation, derived from a simple mass conservation hypothesis", *Bound. Lay. Meteorol.*, **31**(1), 39-49. https://doi.org/10.1007/BF00120033.

Deaves, D.M. (1981), "Computations of wind flow over changes in surface roughness", *J. Wind Eng. Ind. Aerod.*, **7**(1), 65-94. https://doi.org/10.1016/0167-6105(81)90068-4.

Durst, C.S. (1960), "Wind speeds over short periods of time", *Meteor. Mag.*, **89**(1056), 181-187.

Eliasson, I., Offerle, B., Grimmond, C.S.B. and Lindqvist, S. (2006), "Wind fields and turbulence statistics in an urban street canyon", *Atmos. Environ.*, **40**(1), 1-16. https://doi.org/10.1016/j.atmosenv.2005.03.031.

Engineering Science Data Unit (1985), "Characteristics of atmospheric turbulence near the ground, part2: single point data for strong winds (neutral atmosphere)", Item No.85020, London, U.K.

Flay, R.G.J. and Stevenson, D.C. (1988), "Integral length scales in strong winds below 20 m", *J. Wind Eng. Ind. Aerod.*, **28**(1-3), 21-30. https://doi.org/10.1016/0167-6105(88)90098-0.

GB 50009-2012 (2012), "Load code for the design of building structures", China Building Industry Press, Beijing, China.

Giammanco, I.M., Schroeder, J.L. and Powell, M.D. (2013), "GPS dropwindsonde and WSR-88D observations of tropical cyclone vertical wind profiles and their characteristics", *Weather Forecast.*, **28**(1), 77-99. https://doi.org/10.1175/WAF-D-11-00155.1.

Golder, D. (1972), "Relations among stability parameters in the surface layer", *Bound. Lay. Meteorol.*, **3**(1), 47-58. https://doi.org/10.1007/BF00769106.

Good, S.P., Soderberg, K., Wang, L. and Caylor, K.K. (2012), "Uncertainties in the assessment of the isotopic composition of surface fluxes: A direct comparison of techniques using laser-based water vapor isotope analyzers", *J. Geophy. Res: Atmos.*, **117**(D15). https://doi.org/10.1029/2011JD017168.

Grimmond, C.S.B. (1998), "Aerodynamic roughness of urban areas derived from wind observations", *Bound. Lay. Meteorol.*, **89**(1), 1-24. https://doi.org/10.1023/A:1001525622213.

Harper, B.A., Kepert, J.D. and Ginger, J.D. (2010), "Guidelines for converting between various wind averaging periods in Tropical Cyclone Conditions", World Meteorological Organization, WMO/TD, Geneva, Switzerland.

He, Y.C. and Li, Q.S. (2014), "Dynamic responses of a 492-m-high tall building with active tuned mass damping system during a typhoon", *Struct. Control Health Monit.*, **21**(5), 705-720. https://doi.org/10.1002/stc.1596.

He, Y.C., Chan, P.W. and Li, Q.S. (2013a), "Wind profiles of tropical cyclones as observed by Doppler wind profiler and anemometer", *Wind Struct.*, **17**(4), 419-433. https://doi.org/10.12989/was.2013.17.4.419.

He, Y.C., Chan, P.W. and Li, Q.S. (2013b), "Wind characteristics over different terrains", *J. Wind Eng. Ind. Aerod.*, **120**, 51-69. https://doi.org/10.1016/j.jweia.2013.06.016.

He, Y.C., Chan, P.W. and Li, Q.S. (2016), "Observations of vertical wind profiles of tropical cyclones at coastal areas", *J. Wind Eng. Ind. Aerod.*, **152**, 1-14. https://doi.org/10.1016/j.jweia.2016.01.009.

He, Y.C., Chan, P.W. and Li, Q.S. (2017), "Estimation of roughness length at Hong Kong International Airport via different micrometeorological methods", *J. Wind Eng. Ind. Aerod.*, **171**, 121-136. https://doi.org/10.1016/j.jweia.2017.09.019.

He, Y.H., Han, X.L., Li, Q.S., Zhu, H.P. and He, Y.C. (2018a), "Monitoring of wind effects on 600 m high Ping-An Finance Center during Typhoon Haima", *Eng. Struct.*, **167**, 308-326. https://doi.org/10.1016/j.engstruct.2018.04.021.

He, Y.H., Li, Q.S., Zhu, H.P., Han, X.L., He, Y.C. and Li, X. (2018b), "Monitoring of structural modal parameters and dynamic responses of a 600m-high skyscraper during a typhoon", *The Struct. Des. Tall Spec. Build.*, **27**(6), e1456. https://doi.org/10.1002/tal.1456.

Hoebbel, T., Thiele, K. and Clobes, M. (2018), "Wind turbulence parameters from three dimensional full-scale measurements at 344 m high guyed mast site Gartow 2", *J. Wind Eng. Ind. Aerod.*, **172**, 341-350. https://doi.org/10.1016/j.jweia.2017.11.001.

Ishizaki, H. (1983), "Wind profiles, turbulence intensities and gust factors for design in typhoon-prone regions", *J. Wind Eng. Ind. Aerod.*, **13**(1-3), 55-66. https://doi.org/10.1016/0167-6105(83)90128-9.

Jin, T., Tian, Y., Zhang, C. W. and Coit, D.W. (2013), "Multicriteria planning for distributed wind generation under strategic maintenance", *IEEE Transactions on Power Delivery*, **28**(1), 357-367. https://doi.org/ 10.1109/TPWRD.2012.2222936.

Kaimal, J.C., Wyngaard, J.C.J., Izumi, Y. and Coté, O.R. (1972), "Spectral characteristics of surface-layer turbulence", *Quart. J. Royal Meteorol. Soc.*, **98**(417), 563-589. https://doi.org/10.1002/qj.49709841707.

Kareem, A. and Tamura, Y. (2013), "Advanced Structural Wind Engineering", Springer, New York, U.S.A.

Kepert, J.D. (2006), "Observed boundary layer wind structure and balance in the hurricane core. Part I: Hurricane Georges", *J. Atmos. Sci.*, **63**(9), 2169-2193. https://doi.org/10.1175/JAS3745.1.

Knupp, K.R., Walters, J. and McCaul, E.W. (2000), "Doppler profiler observations of Hurricane Georges at landfall", *Geophy. Res. Lett.*, **27**(20), 3361-3364. https://doi.org/10.1029/1999GL011260.

Krayer, W.R. and Marshall, R.D. (1992), "Gust factors applied to hurricane winds", *Bull. Amer. Meteorol. Soc.*, **73**(5), 613-618. https://doi.org/10.1175/1520-0477(1992)073<0613:GFATHW>2.0.CO;2.

Kustas, W.P. and Brutsaert, W. (1986), "Wind profile constants in a neutral atmospheric boundary layer over complex terrain", *Bound. Lay. Meteorol.*, **34**(1-2), 35-54. https://doi.org/10.1007/BF00120907.

Lacy, J.R. and Wyllie-Echeverria, S. (2011), "The influence of current speed and vegetation density on flow structure in two macrotidal eelgrass canopies", *Limnology Oceanography: Fluids Environ.*, **1**(1), 38-55. https://doi.org/10.1215/21573698-1152489.

Lettau, H.H. (1957), "Computation of Richardson numbers, classification of wind profiles, and determination of roughness parameters", *Exploring the Atmosphere's First Mile*, **1**, 328-336.

Li, L., Zhou, Y., Wang, H., Zhou, H., He, X. and Wu, T. (2019), "An analytical framework for the investigation of tropical cyclone wind characteristics over different measurement conditions", *Appl. Sci.*, **9**(24), 5385. https://doi.org/10.3390/app9245385.

Li, Q.S., Li, X., He, Y.C. and Yi, J. (2017), "Observation of wind fields over different terrains and wind effects on a super-tall building during a severe typhoon and verification of wind tunnel predictions", *J. Wind Eng. Ind. Aerod.*, **162**, 73-84. https://doi.org/10.1016/j.jweia.2017.01.008.

Li, Q.S., Zhi, L.H., and Hu, F. (2009), "Field monitoring of boundary layer wind characteristics in urban area", *Wind Struct.*, **12**(6), 553. http://ir.nsfc.gov.cn/paperDownload/1000003913211.pdf.

Masters, F.J., Vickery, P.J., Bacon, P. and Rappaport, E.N. (2010), "Toward objective, standardized intensity estimates from surface wind speed observations", *Bull. Amer. Meteorol. Soc.*, **91**(12), 1665-1682. https://doi.org/10.1175/2010BAMS2942.1.

Melbourne, W.H. (1977), "Probability distributions associated with the wind loading structures", *Institution Engineers (Australia) Civ Eng Trans*, **CE19** (1), 58-67. http://worldcat.org/issn/08190259.

Park, H.W. and Sohn, H. (2006), "Parameter estimation of the generalized extreme value distribution for structural health monitoring", *Probabil. Eng. Mech.*, **21**(4), 366-376. https://doi.org/10.1016/j.probengmech.2005.11.009.

Paulsen, B.M. and Schroeder, J.L. (2005), "An examination of tropical and extratropical gust factors and the associated wind speed histograms", *J. Appl. Meteorol.*, **44**(2), 270-280. https://doi.org/10.1175/JAM2199.1.

Peng, Y.B., Wang, S.F. and Li, J. (2018), "Field measurement and investigation of spatial coherence for near-surface strong winds in Southeast China", *J. Wind Eng. Ind. Aerod.*, **172**, 423-440. https://doi.org/10.1016/j.jweia.2017.11.012.

Powell, M.D., Vickery, P.J. and Reinhold, T.A. (2003), "Reduced drag coefficient for high wind speeds in tropical cyclones", *Nature*, **422**(6929), 279. https://doi.org/10.1038/nature01481.

Rolando, E.V.A. (2008), "Wind directionality: A reliability-based approach", Ph.D. Dissertation, Texas Tech University, U.S.A.

Roth, M. (2000), "Review of atmospheric turbulence over cities", *Quart. J. Royal Meteorol. Soc.*, **126**(564), 941-990. https://doi.org/10.1002/qj.49712656409.

Schroeder, J.L., Edwards, B.P. and Giammanco, I.M. (2009), "Observed tropical cyclone wind flow characteristics", *Wind Struct.*, **12**(4), 349-381. https://doi.org/10.12989/was.2009.12.4.349.

Shiau, B.S. and Chen, Y.B. (2002), "Observation on wind turbulence characteristics and velocity spectra near the ground at the coastal region", *J. Wind Eng. Ind. Aerod.*, **90**(12-15), 1671-1681. https://doi.org/10.1016/S0167-6105(02)00278-7.

Shu, Z.R., Li, Q.S., He, Y. C. and Chan, P.W. (2017), "Vertical wind profiles for typhoon, monsoon and thunderstorm winds", *J. Wind Eng. Ind. Aerod.*, **168**, 190-199. https://doi.org/10.1016/j.jweia.2017.06.004.

Snaiki, R. and Wu, T. (2018), "A semi-empirical model for mean wind velocity profile of landfalling hurricane boundary layers", *J. Wind Eng. Ind. Aerod.*, **180**, 249-261. https://doi.org/10.1016/j.jweia.2018.08.004.

Solari, G. and Piccardo, G. (2001), "Probabilistic 3-D turbulence modeling for gust buffeting of structures", *Probab. Eng. Mech.*, **16**(1), 73-86. https://doi.org/10.1016/S0266-8920(00)00010-2.

Song, L.L., Li, Q.S., Chen, W., Qin, P., Huang, H. and He, Y.C. (2012), "Wind characteristics of a strong typhoon in marine surface boundary layer", *Wind Struct.*, **15**(1), 1-15. http://citeseerx.ist.psu.edu/viewdoc/download?doi=10.1.1.668.811&rep=rep1&type=pdf.

Tamura, Y., Iwatani, Y., Hibi, K., Suda, K., Nakamura, O., Maruyama, T. and Ishibashi, R. (2007), "Profiles of mean wind speeds and vertical turbulence intensities measured at seashore and two inland sites using Doppler sodars", *J. Wind Eng. Ind. Aerod.*, **95**(6), 411-427. https://doi.org/10.1016/j.jweia.2006.08.005.

Thomson, D.J. (1982), "Spectrum estimation and harmonic analysis", *Proceedings of the IEEE*, **70**(9), 1055-1096. https://doi.org/10.1109/PROC.1982.12433.

Tieleman, H.W. (2008), "Strong wind observations in the atmospheric surface layer", *J. Wind Eng. Ind. Aerod.*, **96**(1), 41-77. https://doi.org/10.1016/j.jweia.2007.03.003.

Tse, K.T., Li, S.W., Chan, P.W., Mok, H.Y. and Weerasuriya, A. U. (2013), "Wind profile observations in tropical cyclone events using wind-profilers and Doppler SODARs", *J. Wind Eng. Ind. Aerod.*, **115**, 93-103. https://doi.org/10.1016/j.jweia.2013.01.003.

Vickery, P.J. and Skerlj, P.F. (2005), "Hurricane gust factors revisited", *J. Struct. Eng.*, **131**(5), 825-832. https://doi.org/10.1061/(ASCE)0733-9445(2005)131:5(825).

Vickery, P.J., Wadhera, D., Powell, M.D. and Chen, Y. (2009), "A hurricane boundary layer and wind field model for use in engineering applications", *J. Appl. Meteorol. Climatology*, **48**(2), 381-405. https://doi.org/10.1175/2008JAMC1841.1.

Von Karman, T. (1948), "Progress in the statistical theory of turbulence", *Proceedings of the National Academy of Sciences of the United States of America*, **34**(11), 530. https://doi.org/10.1073/pnas.34.11.530.

Welch, P. (1967), "The use of fast Fourier transform for the estimation of power spectra: a method based on time averaging over short, modified periodograms", *IEEE Transactions on Audio and Electroacoustics*, **15**(2), 70-73. https://doi.org/10.1109/TAU.1967.1161901.

Yu, B. and Gan Chowdhury, A. (2009), "Gust factors and turbulence intensities for the tropical cyclone environment", *J. Appl. Meteorol. Climatology*, **48**(3), 534-552. https://doi.org/10.1175/2008JAMC1906.1.

Zilitinkevich, S.S., Mammarella, I., Baklanov, A. A. and Joffre, S. M. (2008), "The effect of stratification on the aerodynamic roughness length and displacement height", *Bound. Lay. Meteorol.*, **129**(2), 179-190. https://doi.org/10.1007/s10546-008-9307-9.\

AD